Structural and mechanical properties of AlTiTaZr(N) medium entropy films (MEF) obtained by DC magnetron sputtering in dynamic mode

Mohamed El Garah, Sofiane Achache, Alexandre Michau, Frederic Schuster, Frédéric Sanchette

Structural and mechanical properties of AlTiTaZr(-N) medium entropy films (MEF) obtained by DC magnetron sputtering in dynamic mode

Mohamed El Garah,[a, b, *] Sofiane Achache,[a] Alexandre Michau,[c] Frederic Schuster,[b,c] Frederic Sanchette [a,b]

[a] ICD-LASMIS, Université de Technologie de Troyes CNRS, Antenne de Nogent, Pôle Technologique de Sud Champagne, 52800 Nogent, France

[b] NICCI, LRC CEA-ICD LASMIS, UTT, Antenne de Nogent, Pôle Technologique de Sud Champagne, 52800 Nogent, France

[c] Commissariat à l'Energie Atomique et aux énergies alternatives (CEA) Saclay, 91191 Gif-sur Yvette, France

E-mail mohamed.el_garah@utt.fr, frederic.sanchette@utt.fr

Abstract

New AlTiTaZr medium entropy films (MEFs) are elaborated by using direct current magnetron sputtering of four pure metallic targets. The films are deposited in various argon-nitrogen gas mixtures on glass, silicon and sapphire positioned in the center and in the targets axis of a rotating substrates holder. Crystallographic structure evolution, as a function of the nitrogen content, is predicted by calculating the phase selection criteria. The theoretical predicted structures are consistent with X-ray diffraction analysis results. Without nitrogen, the films are amorphous, and by increasing the N_2 content in the gas mixture, they are single phased faces centered cubic (FCC). A {200} preferential growth of AlTiTaZr(-N) films is favored in the targets axis position with increased nitrogen flow rate, whereas those in the center position of substrates holder grow preferentially with {111} planes parallel to the substrates surface.

Hardness and Young's modulus are improved with increasing of the nitrogen flow. The highest values were obtained for those in the targets axis position and reach 24.64 GPa and 148.4 GPa for the hardness and the Young modulus respectively. These films were annealed at 600 °C and 900 °C in vacuum and their thermal stability is discussed.

Keywords: Thin film, medium entropy alloys, thermal stability, PVD

Introduction

Similar to conventional alloys, significant efforts have been recently made to develop high entropy alloys (HEAs). Since the first studies in 2004, they are defined as quasi- or equi-atomic alloys and consist, at least, in five elementary components with atomic percentage ranging from *5* to *35* at. *%* [1-3]. Due to the effect of maximized entropy, these alloys can be single phased solid solutions. Up to date, several investigations have been carried out to explore their physical and chemical features revealing attractive properties and potential uses [4, 5]. Basing on the configurational entropy, alloys having mixing entropy between 1R and 1.5R (R, gas constant) are classed as medium entropy alloys (MEAs). Despite their reduced compositions, 3 or 4 elements, these alloys can also possess interesting structural and mechanical properties [6-8]. High Entropy thin Films (HEFs) have been also developed and used in surface coating technology to improve the durability of materials in extreme environments. They exhibit excellent mechanical and physical properties such as a good wear [9], good corrosion resistance [10] and a high thermal stability [11]. Other properties such as electrical and magnetic have also been reported [12, 13].

Among these different thin films materials, nitride coatings have been widely investigated because of their excellent performances, in particular high hardness and excellent corrosion resistance [14, 15]. Nitride based HEAs coatings can be synthesized in a reactive atmosphere. Generally, without nitrogen, the films have amorphous structures but they can form crystals

upon increasing the nitrogen flow rate [14-17]. The amorphization tendency of these metallic films is a result of the both high mixing entropy and atomic size mismatch. The high mixing entropy improves the solubility of the multi-element compounds preventing then the formation of intermetallic complexes [1, 18, 19]. Nevertheless, the large atomic size mismatch causes a lattice distortion that can favor the growth of amorphous structure.

Various technologies have been used to design and to synthesize this kind of multi-element materials such as laser cladding [20-22], magnetron sputtering [23-29] and others [30-32]. Among them, magnetron sputtering is the most used technique to synthesize these particular alloys in neutral as well as in reactive atmospheres.

Quaternary MEFs could be an alternative to more complex materials. The main objective is to evaluate potentialities of MEFs compared to those of HEAs in terms of mechanical properties, thermal stability and resistance to high temperature oxidation. Kim et al. have studied various compositions of ternary TiTaZr alloys that are used as supports for developing biomaterials [33-35]. Moreover, aluminate alloys have been reported to produce materials with enhanced oxidation resistance. For example, Huang et al. reported that $AlCrFeMo_{0.5}NiSiTi$ and $AlCoFeMo_{0.5}NiSiTi$ films exhibit excellent oxidation resistance that is mainly due to the formation of aluminate oxide on their surfaces [36]. Shen et al. have also investigated the oxidation resistance of $(Al_{0.34}Cr_{0.22}Nb_{0.11}Si_{0.11}Ti_{0.22})_{50}N_{50}$ film. They reported superior oxidation resistance, compared to other nitrides, which is attributed to the protection of a dense Al_2O_3 and to inner Si-rich network [37]. Thanks to attractive properties of aluminum containing materials, we developed AlTiTaZr(-N) alloys, which could be promising for high temperature oxidations resistance. As it is a new composition, their structural and mechanical properties must be first investigated.

In this study, the new quaternary AlTiTaZr(-N) medium entropy films (MEFs) are deposited in dynamic mode on a rotating substrates holder by using magnetron sputtering of four pure

metallic targets. The effects of the substrates position (in the holder's center or in the targets axis) as well as the nitrogen flow rate, on structural, mechanical properties and thermal stability of AlTiTaZr(-N) MEFs are investigated. Deposition is carried out in reactive mode by varying the nitrogen flow rate at constant total pressure.

2. Experimental details

2.1. Deposition

The films are deposited on glass, silicon and sapphire substrates by using magnetron sputtering of pure metallic targets (200 mm in diameter, Figure 1). Substrates are cleaned by subsequent ultrasonication in acetone and ethanol (20 minutes each) followed by drying process with hot air. Afterward, the substrates are ion etched in argon (0.5 Pa) using RF power of 600 watts for 30 minutes.

The targets are first cleaned in argon (0.5 Pa) for 10 minutes before deposition. Discharge current is 1A on each target for 90 minutes. The targets-substrates distance is kept constant at 10 cm. The flow rates ratio $R_{N,}$ which is defined by $R_N=(N_2/Ar+N_2)$ is varied from 0 to 15%. The total pressure is kept constant at 0.3 Pa. No bias or substrates heating is performed during deposition.

2.2. Characterization

All films are analyzed by X-ray diffraction using D8-Advance Bruker diffractometer with CuKα radiation (λ=1.54 Å), θ-2θ (30-90°), step size=0.03 and scan speed = 0.5/s.

The chemical composition of as-deposited films is evaluated by using the scanning electron microscopy (SEM) (Hirow SH-4000M) equipped with an energy dispersive X-ray spectrometer (EDS).

Hardness and Young's modulus are measured by using the Nano Indenter XP, MTS Systems equipped with a three-sided pyramidal diamond tip (Berkovitch indenter). The maximum penetration depth is limited to less than 10% of the film thickness, to avoid the influence of the substrate stiffness. Hundred indents were performed for each sample and an average was obtained.

In order to evaluate the thermal stability of the AlTiTaZr(-N) solid solution at R_N=10%, the films are heated at 600°C or 900°C for two hours in a quartz tube furnace under vacuum. The heating rate is 20°C/s, the temperature is controlled using Carbilite Gero (30°C-3000°C) controller equipped with temperature probe tip inside of the quartz tube.

3. Results and discussion

3.1. Deposition rate and morphology

Figure 2b shows the evolution of the deposition rate as a function of nitrogen content (R_N) in the gas mixture. Films thickness according to the different positions on the sample holder, as a function of R_N, is given figure 2a. By increasing R_N, two phenomena occur; targets' poisoning is favored and argon partial pressure decreases. These both phenomena lead to a decrease of the sputtering rates, as the nitrogen flow increases. As a result, the films deposition rate decreases. It can be observed that, as expected for example at R_N=15%, the deposition rate remains higher in the targets axis; 0.56 µm/h compared to the center position which is 0.47 µm/h.

Fracture cross-sectional SEM images of the films at R_N=0% and R_N=15% for two positions, in the center of substrates holder and in the targets axis, are presented in the figures 3. For both R_N values (0 and 15 at.%), the films deposited in the targets axis seem to be slightly more compact. This is obviously due to the energy of the impinging species on the growing film. Anyway, whatever the position of substrates (Figure 3), the films have compact

morphology. Even if the difference in morphology is not significant, the energy of the impinging species on the growing film in the center of substrate holder is lower because the distance and the angle with the targets axis are much higher.

3.2.Chemical composition

Energy Dispersive Spectroscopy (EDS) is used to evaluate the chemical composition of AlTiTaZr-N films. Effects of both substrate's position and R_N on the film's composition are shown figure 4. When R_N increases, target's poisoning leads to a slight decrease of the metals sputtering rate and consequently a lower metals content. Content of Aluminium (***Al***), which has a strong affinity with the nitrogen, decreases with the evolution of R_N (red curves in Figure 4). Contents of Titanium (***Ti***) and Zirconium (***Zr***) present a quite similar behavior (green and violet curves). Unlike for the other metallic constituents, Tantalum (***Ta***) content seems to remain constant up to R_N = 15% for both positions (blue curves in Figure 4). These results are consistent with the nitrides formation ability, evaluated from ab intio investigations, which show that ***Ta*** is the last metal to be nitrided in our four metal-nitrogen systems [38]. Anyway, Phenomena are quite complex, these four metals do not have the same nitride formation ability and, moreover, targets poisoning leads to change significantly the sputtering yield of each target in different proportions. In our case, nitrogen is first consumed by the metals, which have higher nitride formation ability (***Al***, ***Ti*** and ***Zr***). It is difficult to distinguish the influences of the nitride formation ability and the decrease in sputtering yields during the metallic mode to the reactive mode transition for each binary system. Analyses by Optical Emission Spectroscopy are planned to reach details on phenomena about each target poisoning in different Ar-N_2 atmospheres.

3.3. Structure analysis from phase selection criteria

Phase selection criteria are calculated in order to evaluate the solid-solution formation ability, they have been developed basing on Hume-Rothery rule [39]. Zhang et al. have proposed three criteria for HEAs namely the mixed enthalpy (ΔH_{mix}), the mixed entropy (ΔS_{mix}) and the atomic size mismatch (δ) [40]. HEAs are single phased solid solution if the criteria satisfy $-19 \leq \Delta H_{mix} \leq 5$ KJ/mol, $12 \leq \Delta S_{mix} \leq 17.5$ J/K.mol and $\delta \leq 6.6$ %. Guo et al. have also proposed slightly different limits for these criteria; $-22 \leq \Delta H_{mix} \leq 7$ KJ/mol, $11 \leq \Delta S_{mix} \leq 19.5$ J/K.mol and $\delta \leq 8.5$ % [41]. Recently, Li et al. studied the criteria of multi-components materials obtained by laser-cladding technique [42]. They introduced another criterion depending on the laser energy that influence the formation HEAs solid solutions. Thus, various laser-cladding developed HEAs have been analyzed and the solid solutions are identified when satisfying the following windows; $-17 \leq \Delta H_{mix} \leq 7$ KJ/mol, $10.8 \leq \Delta S_{mix} \leq 16.2$ J/K.mol, $\delta \leq 14$ % and $0.04 \leq K \leq 0.14$ kJ/mm^2 (K is the specific laser energy). From these different reported results, it is clear that the criteria parameters can be influenced by the used technique as well as by the deposition parameters.

To date, concerning the HEFs; a complete study of the phase formation rules lacks. In the present work, different criteria, associated with AlTiTaZr(-N) films as a function of R_N and for both substrates positions, are calculated. Table 1 summarizes the calculated criterions namely ΔH_{mix}, ΔS_{mix}, Ω, δ and the reduced number of valence electrons (e/a). Ω is a thermodynamic parameter representing the competition between enthalpy and entropy of multielement materials [43, 44]. All the parameters were calculated from the following equations:

$\Delta H_{mix} = \sum_{i=1,j>1}^{n} \Delta H_{AB}^{mix} c_i c_j$ (ΔH_{AB}^{mix} is the enthalpy of binary alloys, c_i and c_j are the atomic percent of i^{th} and j^{th} element respectively)

$\Delta S_{mix} = -R \sum_{i=1}^{n} c_i ln\, c_i$; R is the gas constant

$\Omega = \frac{T_m \Delta S_{mix}}{|\Delta H_{mix}|}$; is the thermodynamic parameter taking into account the influence of enthalpy and entropy of elements as well as their melting temperatures (T_m).

$\delta = \sqrt{\sum_{i=1}^{n} c_i (1 - r_i / \sum_{j=1}^{n} c_j r_j)}$; (r_i, r_j, c_i and c_j are the atomic radius and the atomic percent of i^{th} and j^{th} element respectively)

$\frac{e}{a} = \sum_{i=1}^{n} c_i (\frac{e}{a})_i$; where $(e/a)_i$ (electron/atom) is the valence electrons contribution of the i^{th} element with can be obtained from its electronic structure [45].

Basing on these criteria analysis, the films obtained at R_N=10% and 15% could be solid solutions single phased. Zhang et al. have studied $(Al_{0.5}CrFeNiTi_{0.25})N_x$ HEA properties as a function of the nitrogen content in the gas mixture [17]. They analyzed the variation of δ as a function of the nitrogen flow and reported the formation of interstitial solid solutions with δ > 23%. In the present work, Ω and δ are calculated as a function of R_N for both substrates positions (Figure 5). Concerning the films obtained at R_N=10% and 15%, δ and Ω exhibit values in the range of 30.2% to 30.8% (Figure 5a) and 1.2 to 1.4 (Figure 5b) respectively. These results are in good agreement with Zhang's investigations and, according to the reported criteria, it can be expected that crystallized solid solutions are formed at R_N = 10 and 15% and that films deposited at lower nitrogen flow rates are amorphous. Besides, calculations of the valence concentration electron (e/a) have shown that; BCC phase grows preferentially at *e/a* > 2.05, FCC at *e/a* > 1.65 and the mixture (BBC, FCC) at 1.65 < *e/a* < 2.05 [39]. As shown in table 1, AlTiTaZr(-N) films obtained at R_N=10% and 15%, exhibit a *e/a* > 2.05. In those conditions, the films should have FCC structures.

3.4. X-ray diffraction analysis

The XRD patterns of AlTiTaZr(-N) films are shown figure 6. Amorphous structures are formed for both substrates positions at low nitrogen flow rates; R_N=0% and R_N=5% (Figures

6a and 6d). By increasing the nitrogen content in the gas mixture at R_N=10% and 15%, AlTiTaZr(-N) films are clearly FCC single phased (Figures 6b, 6c, 6e and 6f). As expected, the results of X-ray diffraction analysis are consistent with the criteria values discussed in the previous section (3.3). The growth of FCC singles phased films is confirmed at R_N = 10% and 15%.

It is also clearly shown that films deposited at R_N = 10% and 15% present a {111} preferential orientation (figures 6b, 6c and 6e), and that the film deposited at R_N = 15%, positioned in the target axis has a {100} preferential orientation (figure 6f).

These preferential orientations could be explained by the Extended Structure Zone Model (ESZM) [46]. This model explains the film microstructures and the preferential orientations by the mobility of the impinging atoms on the surface of the growing film (Figure 7).

Indeed, when the energy flux, toward the substrate is very low or negligible, the adatoms hit the substrate or the growing thin film with nearly no mobility. As a result, the structure is amorphous (zone Ia and Ib). This is consistent with the film's structures observed at low N/Metal flux ratio (cf. figures 6a and 6d).

When the deposition is carried out at conditions where the energy flux is higher, the adatoms are able to diffuse around and nucleate to form crystalline islands (Zone Ic in figure 7). In this case, adsorbed species cannot diffuse at long distance from one column to another. Therefore, no crystallographic competition between grains occurs in this zone and the texture is random.

Further increase of the energy flux will lead to an intergrain diffusion (zone T in figure 7). This allows the interaction and competition between neighboring grains (columns). Therefore, the films will have a preferential orientation corresponding to the fastest growth direction. Moreover, concerning TiN films, Mathieu et al. [46] have shown that a preferred {111} orientation will occur at low atomic N/Ti flux, and a {200} preferred orientation at higher

atomic N/Ti flux, which would mean that energy of adsorbed species is higher when N/Ti ratio increases [46].

In case of energy flux is high (zone II), the recrystallization during grain growth can occur by ripening, island diffusion or grain boundary migration. Thus, the film will aim for its lowest surface energy. This means that the (200) planes of nitrides films will be parallel to the substrate [47, 48]. Therefore, [200] oriented grains will overgrow the other grains.

From this approach, according to this model, the change from a {111} to {200} preferred orientation for the film deposited on the targets axis with R_N = 15% may be due to the transition from zone T (cf. figure 6c, 6b and 6e) to zone II (cf. figure 6f). Indeed, by increasing the atomic N/Metal flux ratio (cf. figure 6e to 6f) and adatoms mobility associated with the substrates bombardment by positive ions neutralized and reflected on the targets surface [49] (figure 6c to 6f), the {111} to {200} preferred orientation transition is favored.

4. Hardness and Young's modulus of AlTiTaZr(-N) MEF

Hardness and Young's modulus, of the AlTiTaZr-N films are evaluated using nano-indentation. Without nitrogen, hardness is about 6.0 and 8.4 GPa for the films deposited in the center of the substrates holder and in the targets axis respectively (figure 8a). The same films exhibit a Young's modulus of 71.7 and 78.4 respectively. Increasing R_N leads to a significant rise of hardness (Figure 8a) and the higher value of hardness is estimated at 24.6 GPa for the film obtained in the target's axis position at R_N=10% (blue curve, Figure 8a). The modulus is also improved and reaches 148.4 GPa for the same film. In the center position, hardness and Young's modulus are 13.1 GPa and 109.3 GPa respectively. In the center of the substrate holder, the angle of the incident species with the targets axis is about 60°, which leads to lower energy of the growing films bombardment associated with a slightly less compact morphology of the films. As a consequence, this difference in morphology can explain the lower values for coatings deposited in the center of the substrates holder.

Hardness and Young's modulus decrease for the higher nitrogen content (R_N=15%, blue curve figure 8). This result could be associated with the {111} to {200} preferred orientation transition when R_N increases from 10% to 15%. This trend has already been seen by W. J. Chou et al. on TiN films [50]. Indeed, if we assume that AlTiTaZr(-N) films are solid solutions with a NaCl-type structure, the active slip system is {110} <110>. The hardness of the films with (111) preferential orientation would be higher because, for an external force perpendicular to the (111) plans, the resolved shear stress on all the slip systems is zero and plastic deformation is then difficult.

5. Thermal stability

FCC solid solutions of AlTiTaZr(-N) films, obtained at R_N=10%, exhibits highest values of hardness and Young modulus and a {111} preferred orientation for both substrates positions. Figure 9 presents the X-ray diffractograms of the films before and after annealing at 600 and 900 °C for 2 hours. As described above, the films deposited at R_N=10% have a single phased FCC structure and are strongly textured; (111) and (222) planes are clearly detected. After annealing at 600°C and even at 900°C, the structure seems to remain the same, which reveals a high thermal stability (Figure 9a, 9b). After annealing at 900°C, an increase of hardness from 24 GPa to 30.1 GPa of the film deposited in the targets axis position is measured whereas that of film in the center of substrates holder remains constant. The mean grain size of films for each substrates positions at room temperature and after annealing at 900°C are measured from the Scherrer formula with data extracted from MAUD software. The mean grain size of films obtained in the targets axis decreases from 500 nm down to 130 nm after annealing, which can explain the rise of hardness. Anyway, the difference in microstructure evolution after annealing between the two substrates positions is still not clear. Beyond this Hall-Petch type effect, hardness increase by annealing is a phenomenon frequently observed in nanocrystalline materials. It can be linked to a specific threshold grain size of the material.

The reasons are still controversial in the literature, but they are linked to dislocation-grain boundaries interactions. The hardness increase by annealing is often explained by the segregation of the solutes in grain boundaries. Valiev et al. [51] reported that emission of dislocations is suppressed by the elevated solute concentration at grain boundaries. Besides, in these area solutes distribution is not uniform which hinder the emission of the dislocation. Renk et al. [52], meanwhile, reported data from atom probe tomography and mechanical tests, to point out the role of the segregation on strengthening. They concluded that the mechanical behavior of the material is not related to solute amount and the hardening effect, during the annealing, can be attributed to grain boundaries relaxation and to dislocation annihilation.

Conclusion

AlTiTaZr(-N) medium entropy films were successfully synthesized by using the magnetron sputtering of four metallic targets in different Ar-N_2 atmospheres. Substrates are positioned in the center and in the targets axis of a rotating substrates holder. At low nitrogen flow (R_N = 0 and 5%), films are amorphous single phased. The FCC solid solution is observed for higher nitrogen flow ((R_N = 10 and 15%). These results are consistent with the phase selection criteria calculations. It is shown that these structures can be theoretically predicted by calculating the different phase selection criteria.

A preferred orientation of {200} planes parallel to the substrate surface is favored at higher bombardment of the growing film when the substrates are positioned in the targets axis and when the N/Metal ratio increases. Films deposited in the substrates holder center have a {111} texture whatever the nitrogen content in the gas mixture.

Hardness and Young's modulus are the highest for the film obtained in the targets axis position at Rn=10 %; 24.6 GPa and 148.4 GPa respectively. These values are lower when the

substrates are far from the targets axis (in the center of the substrates holder) or if the preferred orientation changes from {111} to {200}.

The structure (FCC solid solution) of the film deposited in the targets axis at R_N=10% seems to be stable after annealing in vacuum at 900°C for 2 hours. Hardening of nitrides films deposited in the targets axis occurred after annealing. This can be explained by the decrease of the mean grain size and by dislocation-grain boundaries interactions after segregation of the solutes in grain boundaries. Further investigations, by transmission electron microscopy are needed to clarify or to confirm these hypotheses.

These results show that it is possible, from selected elements, to obtain interesting performances for these aluminium containing MEF, which can be considered as an alternative to standard HEA films.

Acknowledgements

This works was financially supported by Université de Technologie de Troyes (UTT) and Commissariat à l'Energie Atomique et aux énergies alternatives (CEA).

References

[1] J.-W. Yeh, S.-K. Chen, S.-J. Lin, J.-Y. Gan, T.-S. Chin, T.-T. Shun, C.-H. Tsau, S.-Y. Chang, Nanostructured high-entropy alloys with multiple principal elements: novel alloy design concepts and outcomes, Adv. Eng. Mater., 6 (2004) 299-303.
[2] B. Cantor, I. Chang, P. Knight, A. Vincent, Microstructural development in equiatomic multicomponent alloys, Mater. Sci. Eng. A, 375 (2004) 213-218.
[3] W. Zhang, P.K. Liaw, Y. Zhang, Science and technology in high-entropy alloys, Sci. China Mater., 61 (2018) 2-22.
[4] Y. Zhang, T.T. Zuo, Z. Tang, M.C. Gao, K.A. Dahmen, P.K. Liaw, Z.P. Lu, Microstructures and properties of high-entropy alloys, Prog. Mater. Sci., 61 (2014) 1-93.
[5] B. Gludovatz, A. Hohenwarter, D. Catoor, E.H. Chang, E.P. George, R.O. Ritchie, A fracture-resistant high-entropy alloy for cryogenic applications, Science, 345 (2014) 1153-1158.
[6] Z. Wu, H. Bei, F. Otto, G.M. Pharr, E.P. George, Recovery, recrystallization, grain growth and phase stability of a family of FCC-structured multi-component equiatomic solid solution alloys, Intermetallics, 46 (2014) 131-140.

[7] B. Gludovatz, A. Hohenwarter, K.V.S. Thurston, H. Bei, Z. Wu, E.P. George, R.O. Ritchie, Exceptional damage-tolerance of a medium-entropy alloy CrCoNi at cryogenic temperatures, Nat. Commun., 7 (2016) 10602.
[8] N. Chawake, J. Zálešák, C. Gammer, R. Franz, M.J. Cordill, J.T. Kim, J. Eckert, Microstructural characterization of medium entropy alloy thin films, Scr. Mater., 177 (2020) 22-26.
[9] J.B. Cheng, X.B. Liang, B.S. Xu, Effect of Nb addition on the structure and mechanical behaviors of CoCrCuFeNi high-entropy alloy coatings, Surf. Coat. Tech., 240 (2014) 184-190.
[10] H.-T. Hsueh, W.-J. Shen, M.-H. Tsai, J.-W. Yeh, Effect of nitrogen content and substrate bias on mechanical and corrosion properties of high-entropy films $(AlCrSiTiZr)_{100-x}N_x$, Surf. Coat. Tech., 206 (2012) 4106-4112.
[11] W. Sheng, X. Yang, C. Wang, Y. Zhang, Nano-crystallization of high-entropy amorphous NbTiAlSiWxNy films prepared by magnetron sputtering, Entropy, 18 (2016) 226.
[12] C.-Y. Cheng, J.-W. Yeh, High-entropy BNbTaTiZr thin film with excellent thermal stability of amorphous structure and its electrical properties, Mater. Lett., 185 (2016) 456-459.
[13] P.-C. Lin, C.-Y. Cheng, J.-W. Yeh, T.-S. Chin, Soft magnetic properties of high-entropy Fe-Co-Ni-Cr-Al-Si thin films, Entropy, 18 (2016) 308.
[14] K.-H. Cheng, C.-H. Lai, S.-J. Lin, J.-W. Yeh, Structural and mechanical properties of multi-element $(AlCrMoTaTiZr)N_x$ coatings by reactive magnetron sputtering, Thin Solid Films, 519 (2011) 3185-3190.
[15] P.-K. Huang, J.-W. Yeh, Effects of nitrogen content on structure and mechanical properties of multi-element (AlCrNbSiTiV)N coating, Surf. Coat. Tech., 203 (2009) 1891-1896.
[16] C.-H. Lai, S.-J. Lin, J.-W. Yeh, S.-Y. Chang, Preparation and characterization of AlCrTaTiZr multi-element nitride coatings, Surf. Coat. Tech., 201 (2006) 3275-3280.
[17] Y. Zhang, X.-H. Yan, W.-B. Liao, K. Zhao, Effects of nitrogen content on the structure and mechanical properties of $(Al_{0.5}CrFeNiTi_{0.25})N_x$ high-entropy films by reactive sputtering, Entropy, 20 (2018) 624.
[18] D. Ma, B. Grabowski, F. Körmann, J. Neugebauer, D. Raabe, Ab initio thermodynamics of the CoCrFeMnNi high entropy alloy: Importance of entropy contributions beyond the configurational one, Acta Mater., 100 (2015) 90-97.
[19] Y.J. Zhou, Y. Zhang, Y.L. Wang, G.L. Chen, Microstructure and compressive properties of multicomponent $Al_x(TiVCrMnFeCoNiCu)_{100-x}$ high-entropy alloys, Mater. Sci. Eng. A, 454 (2007) 260-265.
[20] C. Huang, Y. Zhang, J. Shen, R. Vilar, Thermal stability and oxidation resistance of laser clad TiVCrAlSi high entropy alloy coatings on Ti–6Al–4V alloy, Surf. Coat. Tech., 206 (2011) 1389-1395.
[21] H. Zhang, Y. Pan, Y.-Z. He, Synthesis and characterization of FeCoNiCrCu high-entropy alloy coating by laser cladding, Materials & Design, 32 (2011) 1910-1915.
[22] X.-W. Qiu, C.-G. Liu, Microstructure and properties of $Al_2CrFeCoCuTiNi_x$ high-entropy alloys prepared by laser cladding, J. Alloys Compd., 553 (2013) 216-220.
[23] S. Achache, S. Lamri, M.A.P. Yazdi, A. Billard, M. François, F. Sanchette, Ni-free superelastic binary Ti–Nb coatings obtained by DC magnetron co-sputtering, Surf. Coat. Tech., 275 (2015) 283-288.
[24] W.-J. Shen, M.-H. Tsai, Y.-S. Chang, J.-W. Yeh, Effects of substrate bias on the structure and mechanical properties of $(Al_{1.5}CrNb_{0.5}Si_{0.5}Ti)N_x$ coatings, Thin Solid Films, 520 (2012) 6183-6188.
[25] R.-S. Yu, C.-J. Huang, R.-H. Huang, C.-H. Sun, F.-S. Shieu, Structure and optoelectronic properties of multi-element oxide thin film, Appl. Surf. Sci., 257 (2011) 6073-6078.

[26] T.K. Chen, T.T. Shun, J.W. Yeh, M.S. Wong, Nanostructured nitride films of multi-element high-entropy alloys by reactive DC sputtering, Surf. Coat. Tech., 188 (2004) 193-200.
[27] L. Liu, J.B. Zhu, C. Hou, J.C. Li, Q. Jiang, Dense and smooth amorphous films of multicomponent FeCoNiCuVZrAl high-entropy alloy deposited by direct current magnetron sputtering, Materials & Design, 46 (2013) 675-679.
[28] S. Achache, S. Lamri, M.P. Yazdi, A. Billard, M. François, F. Sanchette, Ni-free superelastic binary Ti–Nb coatings obtained by DC magnetron co-sputtering, Surf. Coat. Technol., 275 (2015) 283-288.
[29] S. Achache, A. Alhussein, B. Guelorget, R. Salut, M. François, F. Sanchette, Effect of oxygen addition on microstructure and mechanical properties of quaternary TNTZ superelastic thin films obtained by magnetron sputtering, Mater. Chem. Phys., 217 (2018) 262-269.
[30] C.-Z. Yao, P. Zhang, M. Liu, G.-R. Li, J.-Q. Ye, P. Liu, Y.-X. Tong, Electrochemical preparation and magnetic study of Bi–Fe–Co–Ni–Mn high entropy alloy, Electrochim Acta, 53 (2008) 8359-8365.
[31] T. Yue, H. Xie, X. Lin, H. Yang, G. Meng, Microstructure of laser re-melted AlCoCrCuFeNi high entropy alloy coatings produced by plasma spraying, Entropy, 15 (2013) 2833-2845.
[32] D. Liu, J.B. Cheng, H. Ling, Electrochemical behaviours of $(NiCoFeCrCu)_{95}B_5$ high entropy alloy coatings, Mater. Sci. Tech., 31 (2015) 1159-1164.
[33] W.-G. Kim, H.-C. Choe, Effects of TiN coating on the corrosion of nanostructured Ti–30Ta–xZr alloys for dental implants, Appl. Surf. Sci., 258 (2012) 1929-1934.
[34] H.-J. Kim, Y.-H. Jeong, H.-C. Choe, W.A. Brantley, Surface morphology of TiN-coated nanotubular Ti–25Ta–xZr alloys for dental implants prepared by RF sputtering, Thin solid films, 549 (2013) 131-134.
[35] H.-J. Kim, Y.-H. Jeong, H.-C. Choe, W.A. Brantley, Hydroxyapatite formation on biomedical Ti–Ta–Zr alloys by magnetron sputtering and electrochemical deposition, Thin Solid Films, 572 (2014) 119-125.
[36] P.K. Huang, J.W. Yeh, T.T. Shun, S.K. Chen, Multi-principal-element alloys with improved oxidation and wear resistance for thermal spray coating, Adv. Eng. Mater., 6 (2004) 74-78.
[37] W. Shen, M. Tsai, K. Tsai, C. Juan, C. Tsai, J. Yeh, Y. Chang, Superior oxidation resistance of $(Al_{0.34}Cr_{0.22}Nb_{0.11}Si_{0.11}Ti_{0.22})_{50}N_{50}$ high-entropy nitride, J. Electrochem. Soc., 160 (2013) C531-C535.
[38] C.R. Weinberger, X.-X. Yu, H. Yu, G.B. Thompson, Ab initio investigations of the phase stability in group IVB and VB transition metal nitrides, Comput. Mater. Sci., 138 (2017) 333-345.
[39] M. Calvo-Dahlborg, S.G.R. Brown, Hume-Rothery for HEA classification and self-organizing map for phases and properties prediction, J. Alloys Compd., 724 (2017) 353-364.
[40] Y. Zhang, Y.J. Zhou, J.P. Lin, G.L. Chen, P.K. Liaw, Solid-solution phase formation rules for multi-component alloys, Adv. Eng. Mater., 10 (2008) 534-538.
[41] G. Sheng, C.T. Liu, Phase stability in high entropy alloys: formation of solid-solution phase or amorphous phase, Prog. Nat. Sci.: Mater. I., 21 (2011) 433-446.
[42] Y.F. Juan, J. Li, Y.Q. Jiang, W.L. Jia, Z.J. Lu, Modified criterions for phase prediction in the multi-component laser-clad coatings and investigations into microstructural evolution/wear resistance of $FeCrCoNiAlMo_x$ laser-clad coatings, Appl. Surf. Sc., 465 (2019) 700-714.
[43] Q.-W. Xing, Y. Zhang, Amorphous phase formation rules in high-entropy alloys, Chin. Phys. B, 26 (2017) 018104.

[44] X. Yang, Y. Zhang, Prediction of high-entropy stabilized solid-solution in multi-component alloys, Mater. Chem. Phys., 132 (2012) 233-238.
[45] M. Calvo-Dahlborg, U. Dahlborg, S.G.R. Brown, J. Juraszek, Influence of the electronic polymorphism of Ni on the classification and design of high entropy alloys, J. Alloys Compd., 824 (2020) 153895.
[46] S. Mahieu, P. Ghekiere, D. Depla, R. De Gryse, Biaxial alignment in sputter deposited thin films, Thin Solid Films, 515 (2006) 1229-1249.
[47] B. Rauschenbach, J.W. Gerlach, Texture development in titanium nitride films grown by low-energy ion assisted deposition, Crys. Res. Technol., 35 (2000) 675-688.
[48] A. Wander, I.J. Bush, N.M. Harrison, Stability of rocksalt polar surfaces: An ab initio study of MgO(111) and NiO(111), Phys. Rev. B, 68 (2003) 233405.
[49] F. Sanchette, A. Billard, C. Frantz, Mechanically reinforced and corrosion-resistant sputtered amorphous aluminium alloy coatings, Surf. Coat. Tech., 98 (1998) 1162-1168.
[50] W.-J. Chou, G.-P. Yu, J.-H. Huang, Mechanical properties of TiN thin film coatings on 304 stainless steel substrates, Surf. Coat. Tech., 149 (2002) 7-13.
[51] R.Z. Valiev, N.A. Enikeev, M.Y. Murashkin, V.U. Kazykhanov, X. Sauvage, On the origin of the extremely high strength of ultrafine-grained Al alloys produced by severe plastic deformation, Scr. Mater., 63 (2010) 949-952.
[52] O. Renk, A. Hohenwarter, K. Eder, K.S. Kormout, J.M. Cairney, R. Pippan, Increasing the strength of nanocrystalline steels by annealing: Is segregation necessary?, Scr. Mater., 95 (2015) 27-30.

Figure 1. a) Magnetron sputtering system. b) Chamber, four targets configuration. c) Rotating substrates holder showing the two different substrates positions (center and targets axis).

a)

	R_N (%)	0%	5%	10%	15%
Thickness	Center of substrates holder (µm)	1.75 ± 0.02	1.10 ± 0.02	0.80 ± 0.02	0.71 ± 0.02
	Targets axis (µm)	2.10 ± 0.02	1.80 ± 0.02	1.01 ± 0.02	0.85 ± 0.02

b)

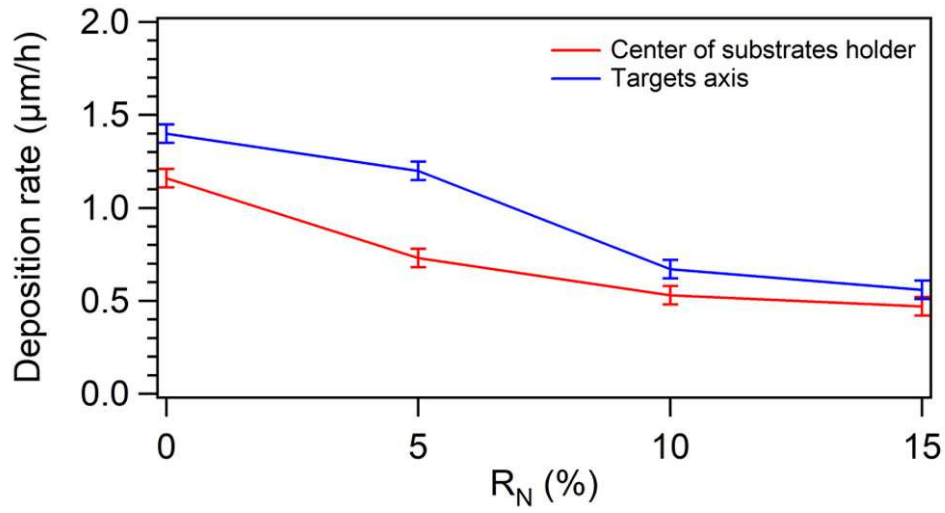

Figure 2. Evolution of thickness (a) and deposition rate (b) of AlTiTaZr(-N) films as a function of R_N for the two positions on the substrates holder.

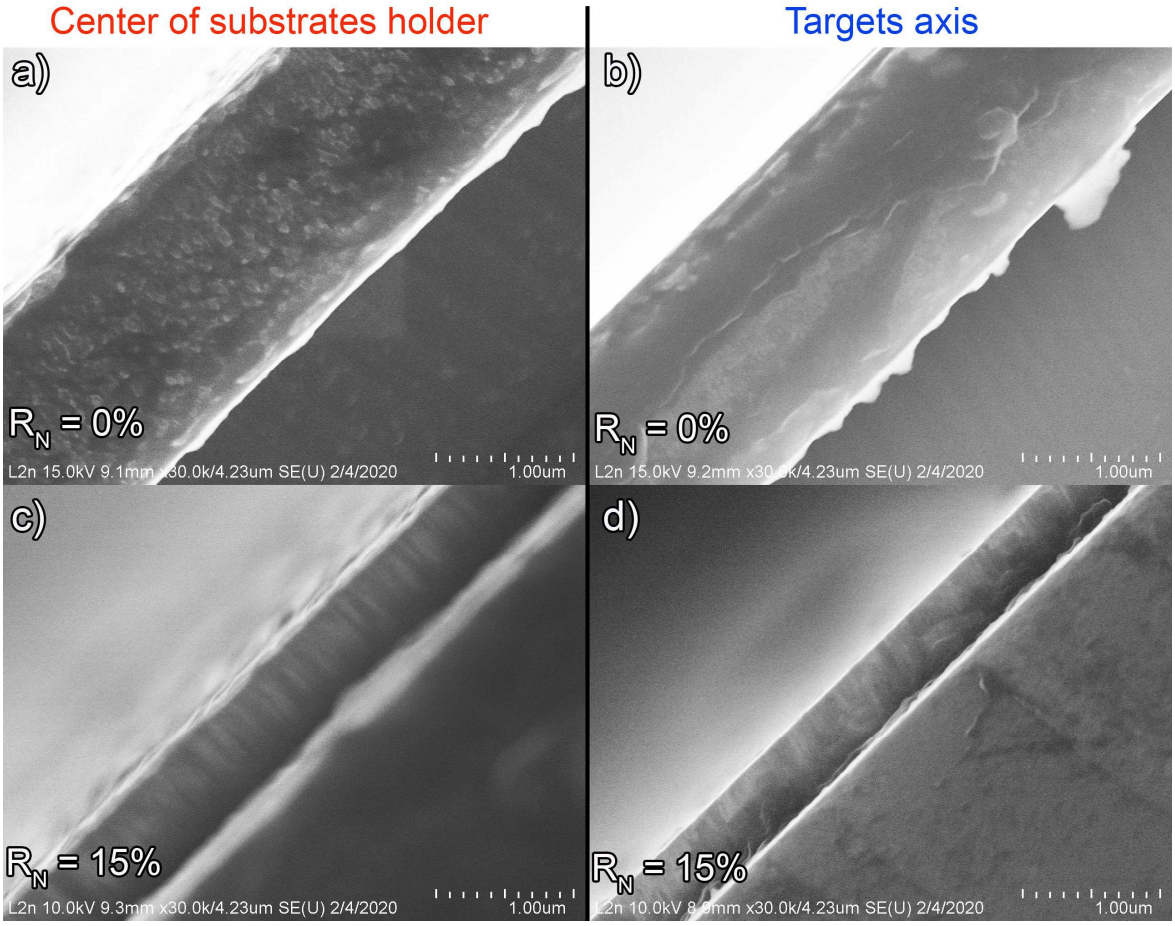

Figure 3. Cross-sectional SEM images of AlTiTaZr(-N) films at R_N = 0% and R_N = 15% for two positions, in the center of substrates holder (a, b) and in the targets axis (c, d) respectively.

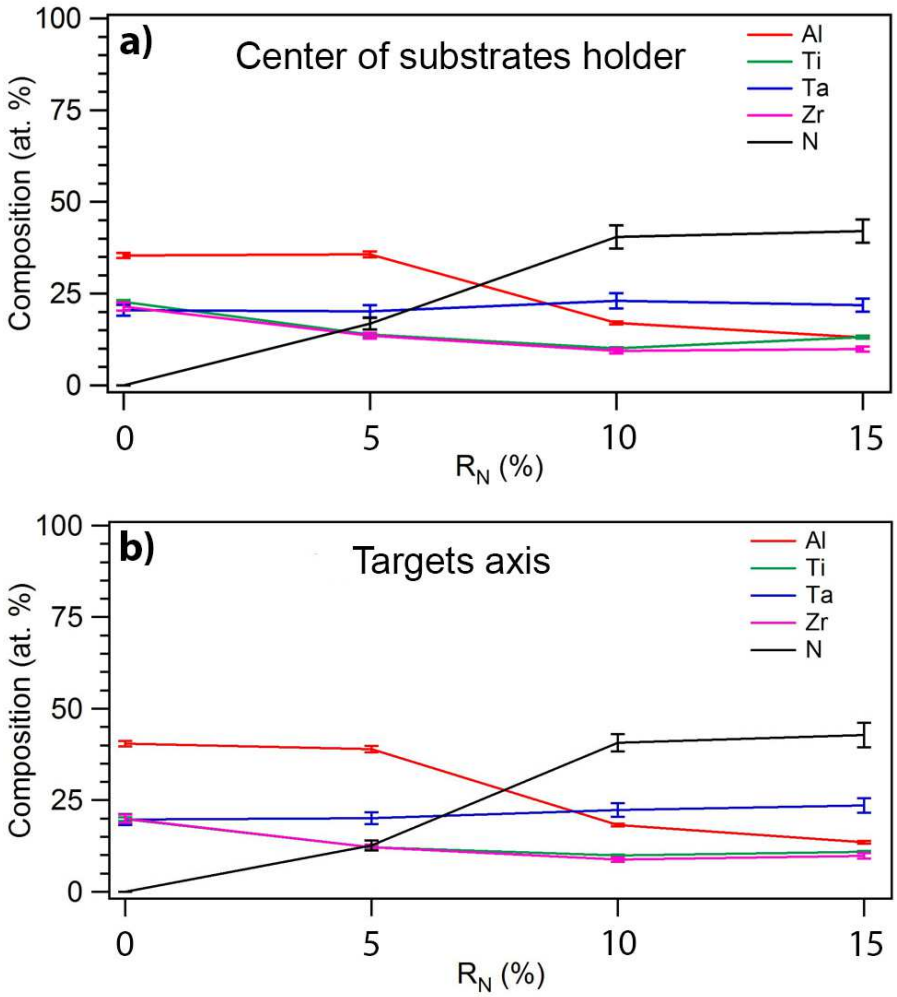

Figure 4. Chemical composition of AlTiTaZr(-N) films as a function of R_N, in the center of sample holder (a) and in the target's axis (b).

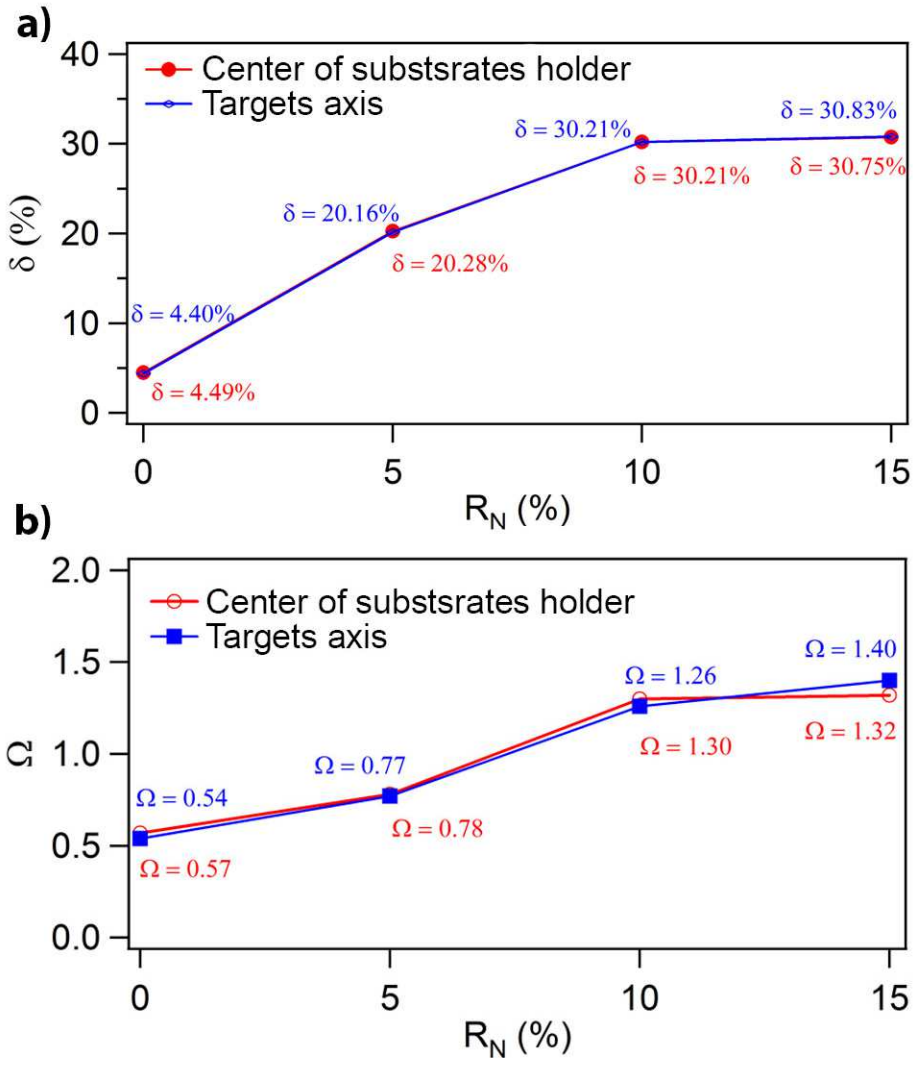

Figure 5. Calculated criteria Ω (a) and δ (b) of AlTiTaZr(-N) films as a function of R_N for the two substrates positions.

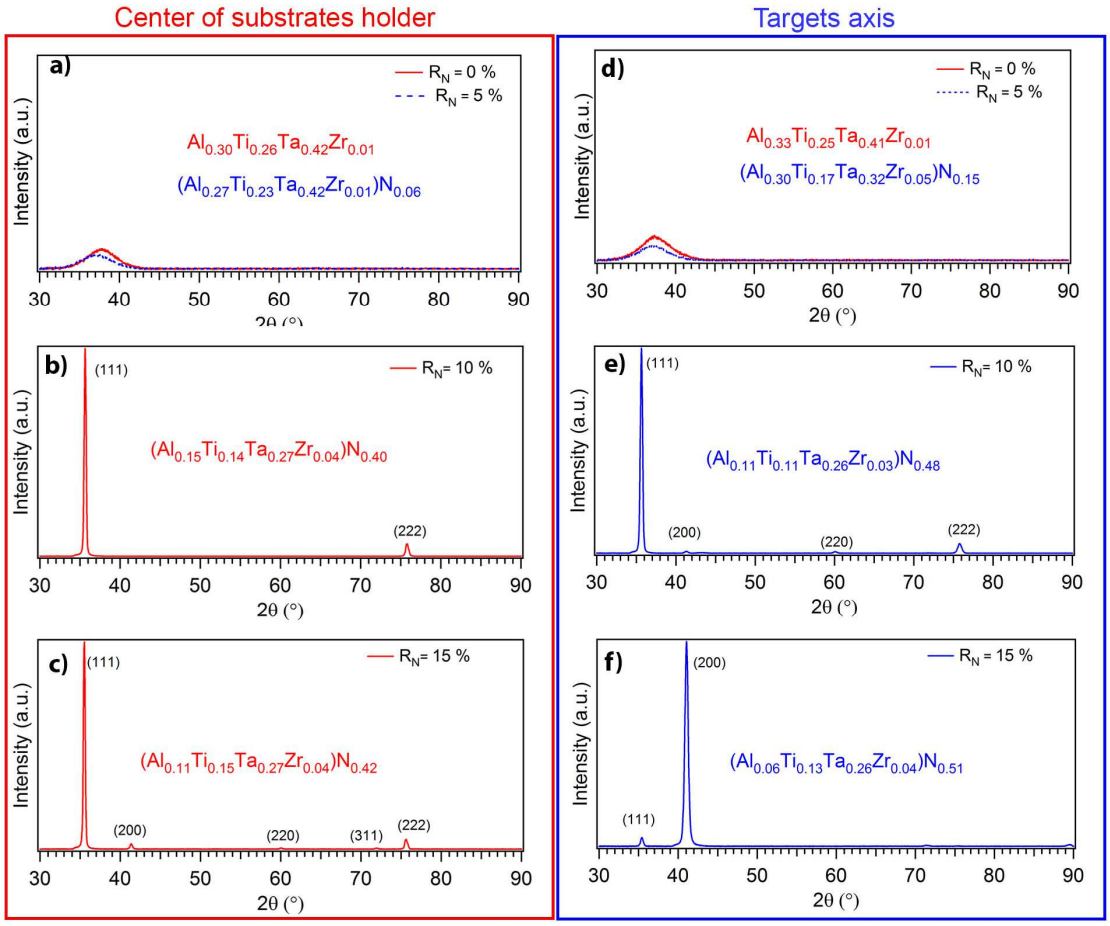

Figure 6. X-ray diffractograms of AlTiTaZr(-N) films at different nitrogen contents in the gas mixture (R_N) (a, d: R_N=0 and 5%; b, e: R_N=10% and c, f: R_N=15%) for two different positions: center of substrates holder (left, a, b and c) and targets axis (right, d, e and f).

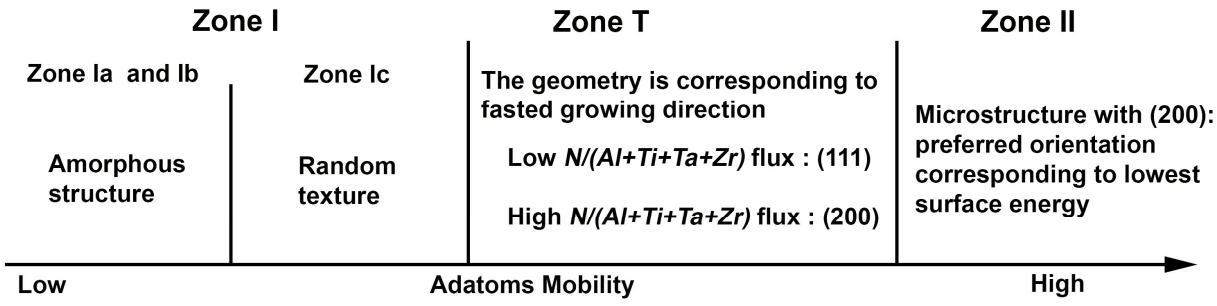

Figure 7. Schema of extended structure zone model of AlTiTaZr(-N) (from [46])

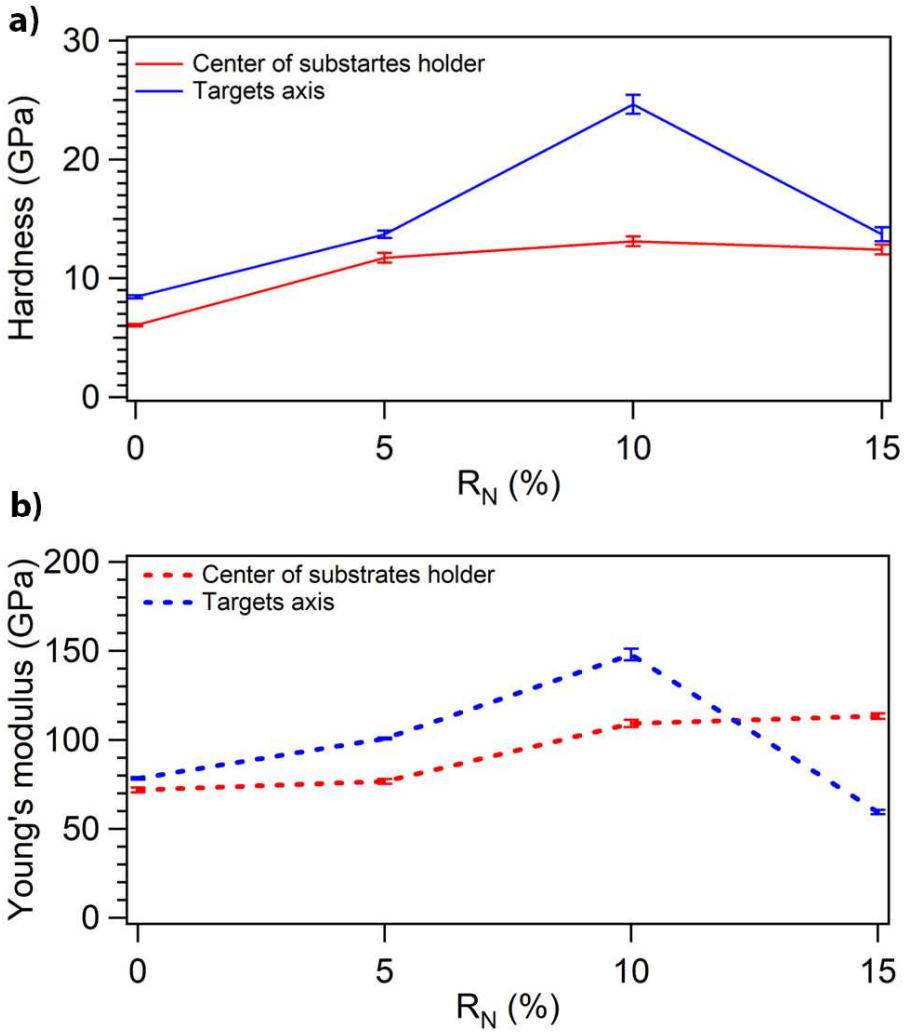

Figure 8. Hardness (a) and Young's modulus (b) of AlTiTaZr(-N) films as a function of the nitrogen content in the gas mixture for two substrates positions; center of substrates holder (red) and in the targets axis (blue).

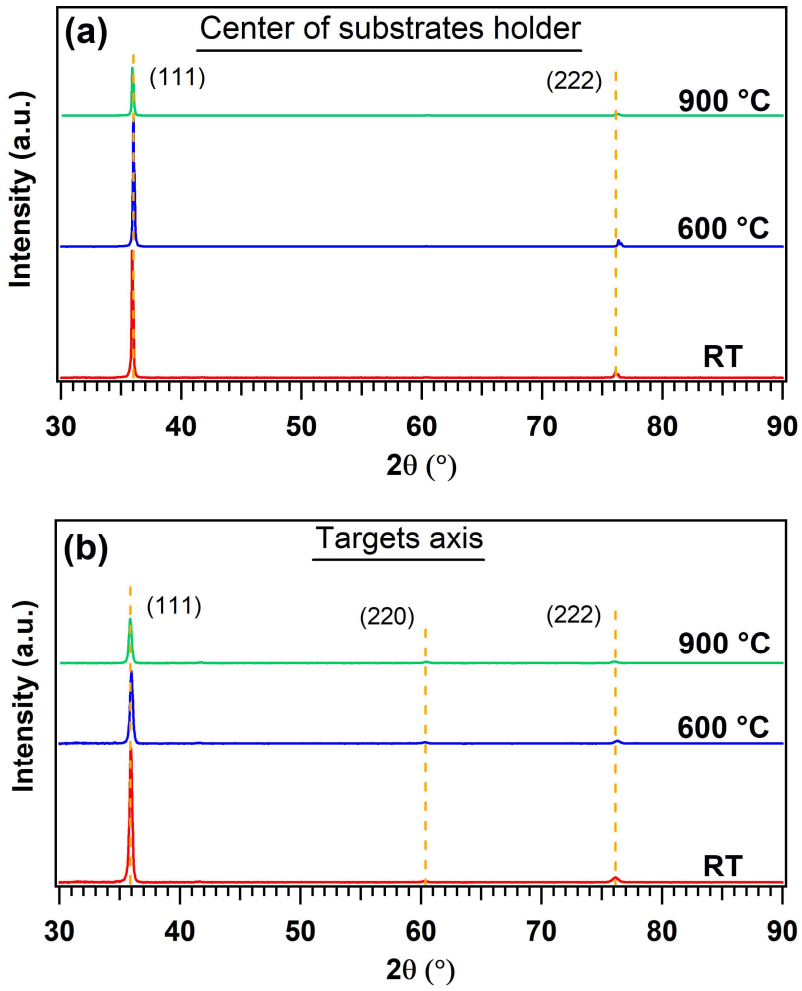

Figure 9. X-ray diffractograms of AlTiTaZr-N films (R_N=10%) annealed at 900 °C. a) Film in the center of substrates holder and. b) Film in targets axis position.

Table 1. Calculated values of ΔH_{mix}, ΔS_{mix}, Ω, δ and *e/a* as a function of of R_N and for two substrates positions.

$R_N = (N_2/N_2+Ar)$	Position	0%	5%	10%	15%
ΔH_{mix} (KJ/mol)	Center of sample holder	*-37.08*	*-25.07*	*-12.17*	*-11.88*
	Target's axis	*-37.12*	*-24.43*	*-12.19*	*-11.26*
ΔS_{mix} (J/K.mol)	Center of sample holder	*11.29*	*12.76*	*12.13*	*12.12*
	Target's axis	*11.05*	*12.47*	*12.09*	*11.99*
Ω	Center of sample holder	*0.57*	*0.78*	*1.30*	*1.32*
	Target's axis	*0.54*	*0.77*	*1.26*	*1.40*
δ ×100(%)	Center of sample holder	*4.49*	*20.28*	*30.21*	*30.75*
	Target's axis	*4.40*	*20.16*	*30.23*	*30.83*
e/a	Center of sample holder	*1.64*	*1.81*	*2.23*	*2.28*
	Target's axis	*1.59*	*1.77*	*2.22*	*2.29*